

# Comparison and extension of methods for acoustic identification of burners

Truffin K. <sup>a,\*</sup> and Poinso T. <sup>b</sup>

<sup>a</sup>*CERFACS, 42 Avenue G. Coriolis, 31057 Toulouse cedex, France*

<sup>b</sup>*Institut de Mécanique des Fluides de Toulouse, Avenue C. Soula, 31400 Toulouse, France*

Cerfacs Ref. : TR/CFD/04/126

---

## Abstract

The prediction and the control of combustion instabilities require the identification of the combustion chamber response. This identification is usually performed by forcing the combustor (for example modulating its inlet velocity) and measuring its response. Two methods may be found in the literature to analyze this response: identification of transfer matrices (ITM) and flame transfer functions (FTF). In ITM approaches, the burner is considered as a "black box" and a two-ports formulation (based on acoustic pressure and velocity perturbations) is used to construct a transfer matrix linking acoustic fluctuations on both sides of the burner. A drawback of this method is that in experiments, the measurement of unsteady pressure and velocity in burnt gases can be a difficult and noisy task. In FTF approaches, pressure measurements are replaced by a global heat release measurement (usually based on optical methods). The heat release fluctuations are then related to the flow velocity modulations at a reference point (usually the combustor inlet) through a transfer function. Both ITM and FTF methods can be used experimentally or numerically but a numerical simulation allows a verification of both concepts: this paper uses a compressible numerical simulation of a forced laminar Bunsen flame to analyze both methods. Results show that FTF approaches lead to an ill-defined problem as soon as the reference point is not close enough to the chamber. This "compactness" limit is quantified here in terms of distance between the reference point and the local chamber. The source of the problem is that FTF approaches correlate heat release fluctuations to velocity oscillations only: extended FTF models are then proposed using the local unsteady pressure as well as the velocity upstream of the flame to predict the heat release oscillations. These models are tested numerically and provides consistent values when the reference point location changes or when upstream and downstream conditions are varied. These extended models are also fully compatible with ITM approaches and provide exactly the same matrices as ITM techniques. These results lead to simple recommendations for experimentalists performing system identification.

*Key words:* Flame transfer functions, identification of transfer matrices, boundary conditions, Large Eddy Simulations

---

---

\* Corresponding author. Tel: +33-5-61-19-3190; fax: +33-5-61-19-3030.  
*Email address:* [truffin@cerfacs.fr](mailto:truffin@cerfacs.fr) (Truffin K.).

## 1 Introduction and configuration

To predict and avoid the instabilities which are sometimes encountered during the design phases of modern combustion chambers [1 – 4], a well-known method is the identification of the combustion chamber response: acoustic waves are introduced in the combustor using loudspeakers or rotating valves and the combustor response is measured.

Two theoretical frameworks are generally used to characterize this response:

- the identification of transfer matrices (ITM) [5 – 9],
- the flame transfer function (FTF) [4, 10 – 15].

In ITM approaches each element of the burner is characterized by a transfer matrix linking the velocity and pressure perturbations at the inlet (index 1) and outlet (index 2) of the element (Fig. 1):

$$\begin{pmatrix} p'_r \\ u'_r \end{pmatrix} = \mathcal{M} \begin{pmatrix} p'_l \\ u'_l \end{pmatrix} \quad \text{with} \quad \mathcal{M} = \begin{bmatrix} M_{11} & M_{12} \\ M_{21} & M_{22} \end{bmatrix} \quad (1)$$

where the four coefficients of  $\mathcal{M}$  are complex numbers. The element containing the flame is treated like all others so that the flame effect is included in the matrix of this element.

FTF models also describe the acoustic propagation upstream and downstream of the burner with transfer matrices like in the transfer matrix but the treatment of the flame element is different: the FTF views the flame as a thin interface separating two elements of the burner (Fig. 2). For this interface the transfer function  $F$  is defined as the ratio of the oscillating heat release  $\dot{\Omega}'_T$  and the unsteady inlet velocity  $u'$ :

$$F(\omega) = \frac{\dot{\Omega}'_T(\omega)}{u'(a, \omega)} \quad (2)$$

where  $\omega$  is the pulsation. Many forms of FTF models can be found: the simplest one is the  $n-\tau$  model [15 – 17] for which the transfer function is approximated by  $F(\omega) = ne^{i\omega\tau}$ . The time  $\tau$  and the interaction index  $n$  characterize respectively the delay and the response intensity between inlet velocity fluctuations  $u'(a, t)$  and total unsteady heat release  $\dot{\Omega}'_T$ :

$$\frac{\gamma - 1}{\rho_1 c_1^2} \dot{\Omega}'_T(t) = S_1 n u'(a, t - \tau) \quad (3)$$

Note that the velocity oscillations are measured at a point  $a$  (usually in the fresh gases upstream of the flame: see Fig. 2) while the heat release fluctuations are integrated over the total combustor volume. The parameters  $n$  and  $\tau$  depend on the pulsation frequency and are building blocks for acoustic codes which predict the overall stability of burners [4, 18, 19].

The whole procedure is limited to low-frequency longitudinal modes.

Both ITM and FTF approaches are used in the literature to process experimental data. ITM approaches require measurements of unsteady pressure in the burnt gases which can be difficult and costly. FTF approaches use measurements of velocity (which are easy using hot wire anemometry) and of unsteady heat release (using for instance CH chemiluminescence signal). Both ITM and FTF can also be used numerically. The objective of this paper is not to discuss the practical aspects of both methods but their theoretical validity. More precisely, the following questions will be addressed:

- A0 - The link between both approaches will be demonstrated to show that both methods are theoretically equivalent.
- A1 - To use FTF methods, an additional condition must be met: the distance  $L^{af}$  between the reference point  $a$  (Fig. 2) and the center of the flame must be small. The validity of this "compactness" assumption is usually investigated by computing the Helmholtz number  $H = \omega L^{af} / c$  which must remain small.  $H$  is also equal to  $2\pi L^{af} / \lambda$  where  $\lambda$  is the acoustic wavelength. In experiments, the reference point is usually not directly placed at the chamber inlet for obvious practical reasons. Moreover the flame itself is often not compact. Therefore an interesting question is to know how large  $H$  can be before results lose their accuracy.
- A2 - To perform measurements with larger  $H$  values, i.e. for points which are away from the chamber inlet plane, can FTF methods be modified?

The reasons motivating these questions are that performing system identification using FTF models should lead to a result which is weakly dependent on the reference point  $a$  and totally independent of the acoustic conditions upstream and downstream of the chamber<sup>1</sup>. The flame transfer function is supposed to characterize a combustion response which does not depend on the details of the acoustic field but only of the fluctuating inlet velocity. If this is not the case the whole procedure provides a transfer function which does not depend only of the combustor but also of all feeding and exhaust lines so that the results are useless: a transfer function measured in a given laboratory for example will not match the transfer function measured in another laboratory for the same burner and combustion chamber (or in the real

---

<sup>1</sup> This condition is satisfied by ITM methods. If properly measured, the matrix  $\mathcal{M}$  of Eq. 1 must depend only on mechanisms occurring within the dashed box (Fig. 1) and not on upstream or downstream conditions.

turbine) if the feeding and exhaust lines differ.

Section 2 first describes the construction of the matrices and the link between both methods (question A0). To be able to answer questions A1 and A2, a prototype configuration is then considered and a full numerical simulation of the compressible reactive flow in this combustor is used to measure all quantities ( $p'_r$ ,  $u'_r$ ,  $p'_l$ ,  $u'_l$ ,  $u'(a)$  and  $\dot{\Omega}'_T$ ) needed to apply ITM or FTF approaches. This prototype corresponds to a simple premixed laminar flame to eliminate sources of uncertainty due to turbulent fluctuations. Its flame response was measured experimentally by Le Helley [20] and numerically by Kaufmann et al. [21] using a specific FTF model which is the  $n - \tau$  model. The present work uses a numerical simulation in which both the reference point (a) and the acoustic conditions on both sides of the chamber can be modified. The  $n - \tau$  parameters are measured for each case and compared. Section 3 briefly describes the numerical method and the technique used for boundary conditions. Section 4 presents the results obtained with the standard  $n - \tau$  model for different positions of the reference point  $a$  and demonstrates that only very low values of  $L^{af}$  allow consistent FTF results. Section 5 shows how FTF models can be extended to provide results which do not depend on the acoustic conditions upstream and downstream of the burner (question A3) and finally section 6 demonstrates that these extended FTF methods are fully equivalent to ITM techniques.

## 2 Methods for system identification

### 2.1 Acoustics in reacting flows

Since acoustics are an essential mechanism controlling combustion instabilities, a brief outline of the derivation of wave equations in reacting flows is first given. A detailed description and discussion of its limits is provided in [3, 4, 22, 23]. For reacting flows at low Mach number the wave equations are derived from the main conservation equations: continuity and momentum. Neglecting viscous and volume forces the starting equations are:

$$\frac{\partial}{\partial t}\rho + \frac{\partial}{\partial x_i}\rho u_i = 0 \tag{4}$$

$$\rho \frac{\partial}{\partial t}u_i = -\frac{\partial}{\partial x_i}p \tag{5}$$

where  $\rho$  is the density,  $u_i$  ( $i = 1, 2, 3$ ) are the velocity components and  $p$  is the pressure. The energy equation is also required:

$$\rho C_p \frac{\partial}{\partial t} T = \dot{\omega}_T + \frac{\partial}{\partial t} p - (\rho C_p u_i) \frac{\partial}{\partial x_i} T \quad (6)$$

where  $C_p$  is the specific heat at constant pressure,  $T$  is the temperature and  $\dot{\omega}_T$  is the heat release rate. Eqs. (4) and (6) may be combined using the ideal gas equation  $p = \rho r T$ . For longitudinal one-dimensional waves, the previous equations may be linearized assuming small acoustic fluctuations ( $\rho'$ ,  $p'$ ,  $u'$ ) compared to the mean flow ( $\rho_0$ ,  $p_0$ ,  $u_0$ ):

$$p(x, t) \approx p_0 + p'(x, t) \quad \rho(x, t) = \rho_0(x) + \rho'(x, t) \quad u(x, t) = u_0(x) + u'(x, t) \quad (7)$$

The integration across a duct of variable cross section (see Fig. 3) leads to the following acoustic model:

$$\rho \frac{\partial}{\partial t} u' = -\frac{1}{\rho_0} \frac{\partial}{\partial x} p' \quad (8)$$

$$\frac{1}{\gamma p_0} \frac{\partial}{\partial t} p' + \frac{1}{S} \frac{\partial}{\partial x} (S u') = \frac{\gamma - 1}{\gamma p_0} \dot{\omega}'_T \quad (9)$$

where  $\gamma$  is the ratio of specific heats,  $\dot{\omega}'_T$  is the fluctuating heat release and  $S(x)$  is the cross section.

## 2.2 Flame transfer function formulations (FTF)

### 2.2.1 Acoustic jump conditions for thin flames

The investigation is limited to piecewise constant duct cross sections with constant mean temperature. If the flame is compact and located in one section ( $x = x_l$  in Fig. 3), all duct elements upstream and downstream of the flame can be merged into one single duct on the left (called "l" here) and one duct on the right (called "r"). The jump conditions at the flame may be formulated by integration of Eqs. (8) and (9) (see Fig. 3) from  $x = x_l^-$  to  $x = x_l^+$  and taking the limit where  $x_l^-$  and  $x_l^+$  go to  $x_l$ :

$$p'(x_l^+) = p'(x_l^-) \quad (10)$$

$$S(x_l^+) u'(x_l^+) - S(x_l^-) u'(x_l^-) = \frac{\gamma - 1}{\gamma p_0} \dot{\omega}'_T \quad (11)$$

where  $\dot{\Omega}'_T = \int_{x_l^-}^{x_l^+} S\dot{\omega}'_T dx$  is the total unsteady heat release in the combustor. These equations show that a compact flame front does not introduce an unsteady pressure jump but a source of volume flow rates. Assuming harmonic variations for any variable  $f$  ( $f' = \hat{f}e^{-i\omega t}$ ), the acoustic pressure and velocity amplitudes are written in duct  $l$ :

$$\hat{p}(x \leq x_l) = A_l^+ e^{ik_l(x-x_0)} + A_l^- e^{-ik_l(x-x_0)} \quad (12)$$

$$\hat{u}(x \leq x_l) = \frac{A_l^+}{\rho_l c_l} e^{ik_l(x-x_0)} - \frac{A_l^-}{\rho_l c_l} e^{-ik_l(x-x_0)} \quad (13)$$

and in duct  $r$ :

$$\hat{p}(x \geq x_l) = A_r^+ e^{ik_r(x-x_l)} + A_r^- e^{-ik_r(x-x_l)} \quad (14)$$

$$\hat{u}(x \geq x_l) = \frac{A_r^+}{\rho_r c_r} e^{ik_r(x-x_l)} - \frac{A_r^-}{\rho_r c_r} e^{-ik_r(x-x_l)} \quad (15)$$

where  $c_l$ ,  $k_l = \omega/c_l$ ,  $\rho_l$ ,  $c_r$ ,  $k_r = \omega/c_r$  and  $\rho_r$  are the sound speeds, the wave numbers and the mean density in sections  $l$  and  $r$  respectively. The unsteady heat release is also supposed to be harmonic:

$$\dot{\Omega}'_T(t) = \hat{\Omega} e^{-i\omega t} \quad (16)$$

### 2.2.2 Transfer matrix for wave amplitudes

A transfer matrix between the wave amplitudes in ducts  $l$  and  $r$  can be derived for Fig. 3 by replacing Eqs. (12) to (16) into the generalized jump conditions (10) and (11):

$$A_r^+ + A_r^- = A_l^+ e^{ik_l l} + A_l^- e^{-ik_l l} \quad (17)$$

$$\frac{S_r}{\rho_r c_r} (A_r^+ - A_r^-) = \frac{S_l}{\rho_l c_l} (A_l^+ e^{ik_l l} - A_l^- e^{-ik_l l}) + \frac{\gamma - 1}{\rho_l c_l^2} \hat{\Omega} \quad (18)$$

Defining  $\Gamma_l = \frac{S_l \rho_r c_r}{S_r \rho_l c_l}$  leads to a matrix  $\mathcal{T}_l$  linking wave amplitudes:

$$\begin{pmatrix} A_r^+ \\ A_r^- \end{pmatrix} = \mathcal{T}_l \begin{pmatrix} A_l^+ \\ A_l^- \end{pmatrix} + \mathcal{O}_l \quad (19)$$

where the transfer matrix  $\mathcal{T}_l$  and the source term due to combustion  $\mathcal{O}_l$  are respectively defined as:

$$\mathcal{T}_l = \frac{1}{2} \begin{pmatrix} e^{ik_l l}(1 + \Gamma_l) & e^{-ik_l l}(1 - \Gamma_l) \\ e^{ik_l l}(1 - \Gamma_l) & e^{-ik_l l}(1 + \Gamma_l) \end{pmatrix} \quad (20)$$

and

$$\mathcal{O}_l = \frac{1}{2} \frac{\rho_r c_r}{S_r} \frac{\gamma - 1}{\rho_l c_l^2} \hat{\Omega} \begin{pmatrix} 1 \\ -1 \end{pmatrix} \quad (21)$$

Using the reflection coefficients at boundaries with Eq. (19):

$$R_l = \frac{A_l^+}{A_l^-} \quad \text{and} \quad R_r = \frac{A_r^+}{A_r^-} e^{2ik_r r} \quad (22)$$

leads to a linear system that is closed if the source term  $\mathcal{O}_l$  (i.e. the unsteady heat release  $\hat{\Omega}$ ) is known.

### 2.2.3 Flame transfer function closures

Many mechanisms are responsible for heat release fluctuations: large scale coherent structures, fluctuations of the equivalence ratio, fluctuations in the strain rate, flame / walls interactions. Therefore, constructing a model for the unsteady heat release  $\hat{\Omega}$  is complex and simplifications are required. Standard FTF approaches do not attempt to account for all these phenomena; they simply assume that the oscillatory combustion is controlled by one mechanism only: the flow velocity modulations at the combustion inlet:

$$\frac{\hat{\Omega}}{\dot{\Omega}_{T,0}} = F(\omega) \cdot \frac{\hat{u}(x_a)}{c_l} \quad (23)$$

where  $\dot{\Omega}_{T,0} = \int \dot{\omega}_T dV$  is the mean integrated heat release.<sup>2</sup> The simplest FTF model ( $n - \tau$ ) was first introduced by Crocco [10, 11]:

$$\hat{\Omega} = S_l \frac{\rho_l c_l^2}{\gamma - 1} n e^{i\omega\tau} \hat{u}(x_a) \quad (25)$$

Eq. (25) states that the time delay between unsteady velocity at a point  $a$  and unsteady heat release is  $\tau$ . The  $S_l \rho_l c_l^2 / (\gamma - 1)$  term is a normalization factor and  $n$  measures the intensity of the response. In practice,  $n$  and  $\tau$  can be measured experimentally [15, 20] or computed [21, 24, 25]. In the low frequency limit, many analytical flame transfer functions can be found in the literature. Most of them are based on a thin flame assumption. The transfer function is often approximated as a first-order system [26]. An analysis of the flame transfer function is realized by Fleifil et al. [27] in the case of axisymmetric configuration and uniform perturbations. Extensions of Ref.[27] to laminar conical flames are investigated by Matsui [28], Ducruix et al. [29] and Schuller et al. [24]. Application of Ref.[27] to V-flames stabilised on a central body are provided by Dowling [30] and Schuller et al. [24]. In complex geometries, Large Eddy Simulations or experiments must replace analytical methods to evaluate the transfer function. Using Eq. (25), Eq. (19) with boundary conditions (22) can then be solved to provide the eigenfrequencies and the growth rates of unstable modes [4].

### 2.3 Identification of transfer matrices (ITM)

ITM approaches link the acoustic perturbations at the inlet (left) and outlet (right) sections of the combustor (Fig. 3) by:

$$\begin{pmatrix} \hat{p}_r \\ \hat{u}_r \end{pmatrix} = \mathcal{M} \begin{pmatrix} \hat{p}_l \\ \hat{u}_l \end{pmatrix} \quad \text{with} \quad \mathcal{M} = \begin{bmatrix} M_{11} & M_{12} \\ M_{21} & M_{22} \end{bmatrix} \quad (26)$$

To close the ITM model, boundary conditions are expressed in terms of primitive variables, typically impedances in sections  $l$  and  $r$  (Fig. 3). Eq. (26) with these boundary conditions is then a linear system providing the eigenfrequencies and growth rates of all modes.

---

<sup>2</sup> Assuming that all the fuel is burnt  $\dot{\Omega}_{T,0}$  may be estimated using the fuel mass flow rate  $\dot{m}_F$  and the heat of reaction  $Q$ :

$$\dot{\Omega}_{T,0} = Q \dot{m}_F \quad (24)$$

The identification (i.e. the determination of the  $M_{ij}$  coefficients) for ITM methods is done as follows. For convenience the notations  $\hat{p}_l$ ,  $\hat{u}_l$ ,  $\hat{p}_r$  and  $\hat{u}_r$  stand in for  $\hat{p}_l(0)$ ,  $\hat{u}_l(0)$ ,  $\hat{p}_r(l+r)$  and  $\hat{u}_r(l+r)$  respectively (Fig. 3). Eq. (26) contains four complex unknowns (the coefficients of the matrix  $\mathcal{M}$ ) and only two equations. A second state must be created to have two more equations. This state must be independent of the first one. Calling these two states (1) and (2), the following system is obtained:

$$\begin{pmatrix} \hat{p}_r^{(1)} \\ \hat{u}_r^{(1)} \\ \hat{p}_r^{(2)} \\ \hat{u}_r^{(2)} \end{pmatrix} \begin{bmatrix} M_{11} & M_{12} & 0 & 0 \\ M_{21} & M_{22} & 0 & 0 \\ 0 & 0 & M_{11} & M_{12} \\ 0 & 0 & M_{21} & M_{22} \end{bmatrix} \begin{pmatrix} \hat{p}_l^{(1)} \\ \hat{u}_l^{(1)} \\ \hat{p}_l^{(2)} \\ \hat{u}_l^{(2)} \end{pmatrix} \quad (27)$$

A criterion to obtain two independent states is that the ratio of the waves going up and downstream of the burner must be different. Two standard methods are used in experiments to do this:

- the so-called *two-load method* [5, 31, 32] consists in modulating the inlet flow for states (1) and (2) and changing the outlet impedance to go from state (1) to state (2), for example by changing the length of the exhaust section downstream of section  $S_r$  (Fig. 3) or varying its impedance while keeping the same geometry,
- the *two source-location method* [5, 31 – 34] consists in modulating the inlet flow for state (1) and the outlet flow for state (2). Usually, state (1) is obtained by forcing the velocity and state (2) by modulating the outlet pressure.

Complete descriptions and analysis of these methods may be found in [5, 31, 35 – 38]. Comparison of boths methods in [32] shows that when determining transfer matrices for a range of frequencies (with transient or random excitations), the 'two-source location' provides better results.

#### 2.4 The link between FTF and ITM methods

For 1D acoustic waves, it is possible to show that FTF approaches can be formulated as a special ITM method, i.e. that a matrix linking states  $l$  and  $r$  can be derived from Eqs. (17) to (21). Such a demonstration has been first detailed by Chu [39], using conservation and kinematical conditions across a flame considered as a discontinuity. Relations linking the acoustic field down- and upstream of the thin flame are also given in [17, 18]. Explicit relations linking the transfer matrix to the  $n - \tau$  model in a Rijke tube are given in

[6, 40] or for a combustion model developed by Keller [41] in a burner with changing area in [17]. A brief demonstration is provided here for a reference point located at the inlet of the right duct ( $x_a = x_l$ ). Starting from FTF formulations (23) linking the unsteady heat release to the velocity fluctuations measured at  $x_a = x_l$  leads to:

$$\frac{\hat{\Omega}}{\hat{\Omega}_{T,0}} = F(\omega) \frac{\hat{u}_l(x_l)}{c_l} \quad (28)$$

Using Eq. (13) for  $x = x_l$ :

$$\frac{\hat{\Omega}}{\hat{\Omega}_{T,0}} = \frac{F(\omega)}{\rho_l c_l^2} (A_l^+ e^{ik_l l} - A_l^- e^{-ik_l l}) \quad (29)$$

Using Eq. (21) and replacing  $\hat{\Omega}$  by expression (29) gives:

$$\mathcal{O}_l = \frac{1}{2} \Gamma_l K F(\omega) \begin{pmatrix} A_l^+ e^{ik_l l} - A_l^- e^{-ik_l l} \\ -A_l^+ e^{ik_l l} + A_l^- e^{-ik_l l} \end{pmatrix} \quad (30)$$

Finally combining Eq. (30) with the jump conditions (19) leads to a matrix relation between wave amplitudes in both sections:

$$\begin{pmatrix} A_r^+ \\ A_r^- \end{pmatrix} = \mathcal{H} \begin{pmatrix} A_l^+ \\ A_l^- \end{pmatrix} \quad (31)$$

with

$$\mathcal{H} = \frac{1}{2} \begin{pmatrix} e^{ik_l l} [1 + \Gamma_l (1 + KF(\omega))] & e^{-ik_l l} [1 - \Gamma_l (1 + KF(\omega))] \\ e^{ik_l l} [1 - \Gamma_l (1 + KF(\omega))] & e^{-ik_l l} [1 + \Gamma_l (1 + KF(\omega))] \end{pmatrix} \quad (32)$$

Eqs. (12) to (15) and Eq. (31) can be combined to obtain the matrix  $\mathcal{M}$  linking the pressure and velocity perturbations at  $x = x_0$  and  $x = x_r$ :

$$\begin{pmatrix} \hat{p}_r \\ \hat{u}_r \end{pmatrix} = \underbrace{\begin{pmatrix} e^{ik_r r} & e^{-ik_r r} \\ \frac{e^{ik_r r}}{\rho_r c_r} & -\frac{e^{-ik_r r}}{\rho_r c_r} \end{pmatrix} \mathcal{H} \begin{pmatrix} 1 & 1 \\ \frac{1}{\rho_l c_l} & -\frac{1}{\rho_l c_l} \end{pmatrix}^{-1}}_{\mathcal{M}} \begin{pmatrix} \hat{p}_l \\ \hat{u}_l \end{pmatrix} \quad (33)$$

Developing Eq. (33) provides an expression for the coefficients of the transfer matrix  $\mathcal{M}$  which depend on the geometry of the burner and on the flame

transfer form  $F(\omega)$  (Table 1). A global transfer matrix  $\mathcal{M}$  can be formulated in a series of  $N$  connected ducts ( $j = 1, N$ ) with one or many flames. Transfer matrices  $\mathcal{T}_j$  and source terms  $\mathcal{O}_j$  can be estimated in each duct section leading to a global matrix  $\mathcal{H}$  given in [4]. This result shows that using a flame transfer formulation is formally equivalent to using a matrix  $\mathcal{M}$  similar to the transfer matrices. It does not mean however that the FTF automatically satisfies criterion A2 listed in the introduction, like ITM methods do. This will be checked in the next sections by using a specific example.

### 3 System identification for a laminar burner

#### 3.1 Numerical tool and boundary conditions

The numerical tool used for the simulations solves the complete compressible Navier-Stokes equations including chemistry in two and three space dimensions [21, 42, 43]. The data structure corresponds to hybrid grids where structured and unstructured meshes can be used.

- High-order schemes are used to minimize errors in the computations of transfer functions. The TTGC scheme implemented here offers third-order in space on hybrid meshes [42].
- Accurate unsteady boundary conditions are required to control the waves reflections and avoid the propagation of non-physical modes. The NSCBC method [44, 45] is used to reach this goal here. The boundary conditions are formulated in terms of characteristic wave variations and allow to control the reflection coefficient  $R$  at the boundary.
- The forcing technique used for the unsteady case is the IWM (Inlet Wave Modulation) method [21]. This technique consists in modulating the acoustic wave entering the domain while letting the wave leaving the domain propagate without reflection.

#### 3.2 Computation of a laminar Bunsen-type flame

The experimental configuration considered for the present investigation consists of a ducted premixed propane / air flame [20]. The conical flame is anchored on the rim of the burner: the flame stabilisation is produced by a perforated plate with 1880 holes of 0.125 mm in diameter each (Fig. 4). In the main longitudinal pipe, honeycomb stitches are placed to ensure laminar flow. The flame is excited by a loudspeaker located in the fresh gases (point A in

Fig. 5). This burner is a proper prototype for studying the flame response to acoustic perturbations:

- It is acoustically compact: the combustion chamber is small compared to the acoustic wave length.
- The geometry is quasi one-dimensional: the whole system including acoustic and combustion can be modelled.
- The flow is laminar so that the flame response can be studied in the absence of uncertainties related to turbulent combustion models.

The computational domain given in Fig. 5 is reduced to a half burner including one hole of the perforated plate (Fig. 4). The axisymmetrical computational mesh allows the flame to be properly resolved on this mesh (10515 nodes). The laminar flame thickness is 0.3 mm while the typical mesh size is 0.043 mm. The chemical scheme used for this study takes into account five species ( $C_3H_8$ ,  $O_2$ ,  $CO_2$ ,  $H_2O$  and  $N_2$ ) and a single step reaction modeled using an Arrhenius law:

$$q = A \left( \frac{\rho Y_{C_3H_8}}{W_{C_3H_8}} \right)^{n_F} \left( \frac{\rho Y_{O_2}}{W_{O_2}} \right)^{n_O} \exp \left( -\frac{E_a}{RT} \right) \quad (34)$$

where  $q$  is the rate of the single reaction,  $Y_{C_3H_8}$ ,  $Y_{O_2}$ ,  $W_{C_3H_8}$  and  $W_{O_2}$  are respectively the mass fractions and the molecular weights of propane and oxygen. The pre-exponential constant is  $A = 3 \cdot 10^{10}$  cgs, the mass fraction exponents are  $n_F = 0.85$  and  $n_O = 0.50$  and the activation energy is  $E_a = 31100 \text{ cal.mol}^{-1}$ . These parameters are fitted to produce correct flame speeds in the range of equivalence ratios of Le Helley's experiment. The acoustic modulation at the inlet is kept to 10% of the mean velocity ( $4 \text{ m.s}^{-1}$ ) and remains within the linear acoustic domain. Fig. 6 shows four snapshots of the flame during one cycle at 500 Hz. The flame position changes from 1.8 mm to 2.2 mm. The relative variations of the heat release rate are 12% while the relative inlet velocity changes are 10%.

#### 4 Results using a specific FTF model: the $n - \tau$ approach

The regime investigated both numerically and experimentally corresponds to a flow rate of  $10.86 \text{ g.s}^{-1}$  (for the whole burner) and an equivalence ratio of 1.2. The inlet temperature is 300 K and the pressure is 1 bar. In the experiment of Le Helley, a hot wire is placed 2.9 cm (point C in Fig. 4) upstream of the flameholder to measure the velocity  $u'(t)$ . Integral heat release fluctuations are measured by a photo multiplier. In the calculation temporal signals of integrated heat release  $\hat{\Omega}'_T$  and velocity  $u'(a, t)$  are stored. The  $n$  and  $\tau$  parameters can then be obtained using Eq. 25 and the Fourier transform of these temporal

signals. Calculations were performed for different reflection coefficients at the outlet (point E in Fig. 5) at a forcing frequency of 500 Hz.

Fig. 7 shows the mode structure measured in the simulation inside the upstream duct ( $x < 0$  mm). Simply observing the shapes of the modes in Fig. 7 demonstrates that choosing the location for the reference point is critical: obviously  $u'(a, t)$  will change significantly when  $x_a$  varies between  $-600$  and  $0$  mm and the transfer function parameters  $n$  and  $\tau$  will also vary. Various outlet reflection coefficients  $R_E$  have been tested at  $x = 8$  mm (point E) from almost non reflecting ( $R_E = 0.05$ ) to fully reflecting ( $R_E = 1$  or  $p'(x_E) = 0$ ).

Three reference points were tested to evaluate the velocity fluctuations (Fig. 5):

- point D is at the chamber inlet plane,
- point C is 2.9 cm upstream of the chamber inlet. This is the point used for measurements,
- point B is 30 cm upstream of the chamber inlet. This point is chosen so as to avoid singularities, like pressure or velocity extrema as seen in Fig. 7.

The Helmholtz number  $H$  can be estimated at each point (B, C or D) using the distance  $L^{af}$  (Fig. 2) between the reference point ( $x_B, x_C$  or  $x_D$ ) and the center of the flame (located at  $x_f \approx x_{tf}/2 = 1$  mm on Fig. 5). The value for  $H$  (given on Fig. 5) is  $9.0 \cdot 10^{-3}$  at point D and 2.7 at point B. The values for the transfer function parameters are given in Fig. 8. The transfer function parameters calculated using point D seem to be independent of the reflection coefficient. On the contrary, the values of  $n$  and  $\tau$  obtained using points B or C present a strong dependance with  $R_E$ .  $n$  varies non linearly within a factor 1.8 for point B and 1.4 for point C when the outlet reflection coefficient  $R_E$  varies while a maximum deviation of 36 % for point B and 16% for point C are observed for  $\tau$ . When the reference point is C like in the experiment and the outlet reflection coefficient is zero like in the experiment, the computation recovers both the values of  $n$  (4.3) and  $\tau$  (0.47 ms). However, as soon as the outlet reflection changes, results for  $n$  and  $\tau$  change for reference points B or C showing that criteria A2 is not satisfied: changing the reference point from B to C or D changes both  $n$  and  $\tau$ . The only situation which provides results which are independent of the boundary conditions is to use point D (the closest point to the chamber inlet) as a reference point. In this case results are independent of the outlet reflection coefficient  $R_E$ . These results show that the  $n - \tau$  model is not well adapted when the point used to measure velocity oscillations is too far from the flame. In that situation, the reference velocity oscillations  $u'(a, t)$  are disturbed by the reflecting waves imposed by the geometry. This conclusion is not surprising since the initial Crocco model assumed the flame to be compact, i.e. that the distance between reference point and flame must be small compared to the acoustic wavelength. The calculation of the Helmholtz number shows that very small values ( $H \propto 10^{-3}$ )

are required to obtain values of phase and gain of the flame response which are independent of the outlet reflection coefficient. The present results help to quantify this constraint: for points B and C with  $H$  values of 2.7 and 0.27 respectively, the "compact" assumption is obviously not valid. However at point D which is close to the flame ( $H = 9 \cdot 10^{-3}$ ), the standard  $n - \tau$  model seems to perform reasonably. This is however a significant difficulty for experimental studies where the reference point is rarely very close to the flame for practical reasons.

## 5 Extended FTF models

The essential drawback of the  $n - \tau$  model evidenced in the previous sections comes from the fact that it tries to correlate heat release perturbations to velocity perturbations only. In this section extended FTF models are proposed to build a consistent formulation which can be used for any location of the reference point. These models are formulated using the local unsteady pressure and velocity measured upstream of the flame:

$$\frac{\hat{\Omega}}{\hat{\Omega}_{T,0}} = F_u(\omega) \frac{\hat{u}_l(x_a)}{c_l} + F_p(\omega) \frac{\hat{p}_l(x_a)}{p_l} e^{i\omega\tau_p} \quad (35)$$

In the specific case of the  $n - \tau$  model  $F_u(\omega) = A_u e^{i\omega\tau_u}$  and  $F_p(\omega) = A_p e^{i\omega\tau_p}$  so that:

$$\frac{\hat{\Omega}}{\hat{\Omega}_{T,0}} = A_u \frac{\hat{u}_l(x_a)}{c_l} e^{i\omega\tau_u} + A_p \frac{\hat{p}_l(x_a)}{p_l} e^{i\omega\tau_p} \quad (36)$$

where the unsteady velocity, pressure and heat release are scaled respectively by the sound speed  $c_l$ , the mean pressure  $p_l$  and Eq. (36) contains four unknowns  $A_u$ ,  $A_p$ ,  $\tau_u$  and  $\tau_p$  which depend on the point where velocity and pressure fluctuations are measured. These parameters may be determined by using two sets of independent measurements like for ITM methods.<sup>3</sup> As explained in Section 2.3 different techniques may be used to obtain two independent states. Here states (1) correspond to simulations with minimum reflection at boundaries (Table 2). States (2) are obtained by modifying the location of the

---

<sup>3</sup> If the transfer matrix  $\mathcal{M}^{aD}$  between the reference point ( $a$ ) and the burner mouth (point D in Fig. 5) is known analytically, then one state can be sufficient: in this case, the velocity signal at the burner mouth  $\hat{u}_D$  can be obtained by  $\hat{u}_D = \mathcal{M}_{21}^{aD} \frac{\hat{p}_a}{\rho c} + \mathcal{M}_{22}^{aD} \hat{u}_a$  and the standard  $n - \tau$  model can be applied by determining  $n$  and  $\tau$  such that  $\hat{\Omega} = n e^{i\omega\tau} \hat{u}_D$ . However in many cases, the transfer matrix  $\mathcal{M}^{aD}$  is not known in which case two states are needed.

acoustic source and/or by increasing the reflection coefficient at one boundary (right or left). The resulting states are classified in three test cases (Table 2):

- Case 1: for states (1) and (2) the velocity is modulated on the left side (upstream of the flame) and the outlet reflection coefficient  $R_E$  of state (2) is changed.
- Case 2: states (1) and (2) are obtained by applying forcing on the right and left sides respectively and by increasing the outlet impedance of state (2).
- Case 3: states (1) and (2) are obtained by applying forcing on the left and right sides respectively and by increasing the inlet impedance of state (2).

The calculations described in section 4 are used to determine the parameters of the extended  $n - \tau$  model. The velocity and pressure fluctuations are measured at points B ( $x = -300$  mm), C ( $x = -29$  mm) and D (chamber inlet). The coefficients are displayed in Figs. 9 to 11 at the forcing frequency 500 Hz. For case 1 care is taken to select different load impedances between states (1) and (2): indeed, if the outlet reflection coefficients  $R_E$  used for states (1) and (2) are too close, the two states become linearly dependent leading to an ill-posed formulation. Typically  $R_E$  was set to 0.05 for state (1) and varies between 0.5 and 1 for states (2).

For the three points (B, C and D) cases 1, 2 and 3 provide almost constant values when the reflection coefficient  $R_E$ . Any upstream reference point can be chosen (point B in Fig. 9, C in Fig. 10 or D in Fig. 11) and provides results for  $A_u$ ,  $A_p$ ,  $\tau_u$  and  $\tau_p$  which do not depend on the upstream or downstream boundary conditions ( $R_A$  or  $R_E$ ).

An explanation for the deviations obtained with the standard  $n - \tau$  model (section 4) is also possible when comparing the amplification factors  $A_u$  and  $A_p$ . Using point B or C which are located respectively 300 and 29 mm upstream of the chamber  $A_u$  and  $A_p$  values are of the same order:  $A_p/A_u \approx 0.16$  to  $0.33$  in Figs. 9 and 10 (a),(c). This does not mean that the pressure fluctuations influence the combustion but that at this point both quantities  $u'$  and  $p'$  are needed to describe the response of the flame to acoustic perturbations. Using point D which is in the inlet plane of the chamber  $A_p$  is much lower than  $A_u$ :  $A_p/A_u \approx 0.04$  in Fig. 11(a),(c): at the chamber inlet the effect of pressure modulations on combustion is negligible confirming the steering idea of the  $n - \tau$  model as stated by Crocco [10, 11]. However,  $A_p$  does not go exactly to zero for low values of  $H$  (points close to the burner mouth) showing the limits of the "compactness" assumption used in most FTF approaches. Evaluating  $A_p$  is therefore a useful exercise to verify the validity of FTF measurements.<sup>4</sup>

---

<sup>4</sup> Note that at Point D the error in the evaluation of the delay  $\tau_p$  can reach 15% in Fig. 11(d) because  $A_p$  is very small: the flame is almost insensitive to pressure at point D and the measurement of a delay is noisy.

## 6 Equivalence of ITM and extended FTF methods

It is possible to demonstrate that extended FTF models are fully compatible with ITM approaches by performing the following test (Fig. 12): consider any point located upstream of the chamber ( $x < 0$  in Fig. 5); perform first system identification using ITM methods between this point and the outlet of the chamber (point E in Fig. 12) to obtain a transfer matrix  $\mathcal{M}$  between the reference point and the outlet point E. Second, measure the coefficients  $F_u(\omega)$  and  $F_p(\omega)$  using extended FTF methods and from these coefficients, use Table 3 to construct a second transfer matrix  $\mathcal{M}'$  between the reference point and the outlet point E.<sup>5</sup> These two matrices should be the same. This is demonstrated in Fig. 13 which gives the amplitude and phase of the four complex coefficients  $M_{ij}$  obtained by ITM methods (circles) and by extended FTF models (solid line).

The excellent agreement obtained for all values of the reference point between point D ( $x = 0$  mm) located at the chamber inlet and point B ( $x = -300$  mm) located far upstream of the chamber shows that extended FTF methods are indeed equivalent to ITM approaches. This has important consequences: while the previous sections had shown that standard FTF models were reliable only for very small values of the Helmholtz number ( $H < 10^{-2}$ ), it is now clear that extended FTF models can provide consistent results for all values of  $H$  and are also fully compatible with ITM approaches. Experimentally, this means that ITM approaches (which are often difficult to use) can be replaced by extended FTF methods which are sometimes simpler to implement. It will however require that experimentalists measure not only  $u'$  at the reference point but also  $p'$  (in the fresh gases).

## 7 Conclusion

In this paper, the two standard methods for system identification of combustors have been compared:

- ITM methods [17, 33] in which pressure and velocity perturbations upstream and downstream of the flame are correlated through a single transfer matrix  $\mathcal{M}$ ,

---

<sup>5</sup> When the reference point is B or C (Fig. 5), the section change at  $x = -12$  mm must also be accounted for. Moreover, when the reference point is close to a pressure or velocity node in the upstream duct, it is more convenient to determine the amplitudes of the up and downstream waves travelling in the duct as discussed in [5, 8, 33]. Reconstructing the matrix  $\mathcal{M}$  from these waves is simple using Eq. (9) in Ref.[8].

- FTF methods in which the global unsteady heat release is correlated to the upstream velocity oscillations at a point (a).

It was first shown that using FTF methods are formally equivalent to using a simplified transfer matrix. However, a simulation of a laminar flame using various reference points (a) and various outlet reflection coefficients was performed to demonstrate that FTF models can not be used reliably when the reference point is not very close to the chamber inlet: in those cases, the gain and phase of the transfer function  $F(\omega)$  depend both on the point location and on the acoustic states upstream and downstream of the chamber. Typically, the distance between reference point and chamber inlet must be such that the Helmholtz number  $H = \omega L^{af}/c$  is smaller than 0.01 to obtain consistent results. In practice, this would imply that combustors transfer functions measured or computed for reference points which are not located close enough to the chamber are not intrinsic parameters of the chamber but depend also on upstream and downstream conditions: a combustion chamber installed in a laboratory environment, in which upstream and downstream acoustic conditions are different from the real machine, will have a different transfer function so that the laboratory measurements become useless for the real device.

To overcome this difficulty, ITM methods can be used but these methods are sometimes difficult to implement experimentally because precise acoustic measurements are required in the burnt gases. The alternative solution proposed in this work is to extend FTF methods by expressing the unsteady reaction rate as a function of both local velocity and pressure oscillations. It was shown that these techniques provides consistent results: the transfer function obtained by the extended  $n - \tau$  model does not depend on the acoustic conditions upstream and downstream of the burner. Moreover the transfer matrix which can be deduced from extended FTF formulations is exactly the one obtained by ITM techniques. These results suggest that experimental and computational studies of flame transfer functions could be performed with this extended methods: in practice, this would mean measuring not only the unsteady velocity at the reference point (done usually with hot wire anemometry) but also the unsteady pressure (which is easy at the reference points because they are located in fresh gases).

## References

- [1] T. Poinsot, A. Trouvé, D. Veynante, S. Candel and E. Esposito, *J. Fluid Mech.* 177 (1987) 265-292.
- [2] S. Candel, *Proc. Combust. Institute* 24 (1992) 1277-1296.
- [3] D. G. Crighton, A. Dowling, M. Heckl, F. Leppington and J. Williams, *Modern methods in analytical acoustics*, Springer Verlag, 1992.
- [4] T. Poinsot and D. Veynante, *Theoretical and Numerical Combustion*, R.T. Edwards, 2001.
- [5] M. Åbom, *Mechanical Systems and Signal Processing* 5 (2) (1991) 89-104.
- [6] W. Polifke and C. O. Paschereit, *Determination of thermo-acoustic transfer matrices by experiment and computational fluid dynamics*, ERCOFTAC bulletin 38, 1998.
- [7] C. O. Paschereit and W. Polifke, *Characterization of lean premixed gas-turbine burners as acoustic multi-ports*, APS / DFD bulletin, 1997.
- [8] C. Pankiewicz, A. Fischer, C. Hirsch and T. Sattelmayer, *9th AIAA/CEAS Aeroacoustics Conference & Exhibit*, 2003.
- [9] C. O. Paschereit, P. Flohr and B. Schuermans, *39th AIAA/ASME*, 2001-0484, 2001.
- [10] L. Crocco, *J. American Rocket Society* 21 (1951) 163-178.
- [11] L. Crocco, *J. American Rocket Society* 22 (1952) -.
- [12] W. Krebs, P. Flohr, B. Prade and S. Hoffmann, *Combust. Sci. Tech.* 174 (2002) 99-128.
- [13] D. Bernier, S. Ducruix, F. Lacas, S. Candel, N. Robart and T. Poinsot, *Combust. Sci. Tech.* 175 (2003) 993-1013.
- [14] W. S. Cheung, G. J. M. Sims, R. W. Copplestone, J. R. Tilston, C. W. Wilson, S. R. Stow and A. P. Dowling, *ASME Paper*, 2003-GT-38219, 2003.
- [15] H. Buchner, C. Hirsch and W. Leuckel, *Combust. Sci. Tech.* 94 (1993) 219-228.
- [16] B. Varoquie, J. Légier, F. Lacas, D. Veynante and T. Poinsot, *Proc. Combust. Institute* 29 (2002) 1965-1970.
- [17] B. Schuermans, W. Polifke and C. O. Paschereit, *Int'I Gas Turbine & Aeroengine Congress & Exposition*, ASME paper 99-GT-132., 1999.
- [18] A. P. Dowling, *J. Sound Vib.* 180 (4) (1995) 557-581.
- [19] W. Krebs, B. Prade, S. Hoffmann, S. Lohrmann and H. Buchner, *ASME Paper*, 2002-GT-30065, 2002.

- [20] H. J. Merk, *Proc. Combust. Institute* 6 (1956) 500-512.
- [21] M. Fleifil, A. M. Annaswamy, Z. A. Ghoneim and A. F. Ghoneim, *Combust. Flame* 106 (1996) 487-510.
- [22] Y. Matsui, *Combust. Flame* 43 (1981) 199-209.
- [23] S. Ducruix, D. Durox and S. Candel, *Proc. Combust. Institute* 28 (2000) 765-773.
- [24] T. Schuller, D. Durox and S. Candel, *Combust. Flame* 134 (2003) 21-34.
- [25] A. P. Dowling, *J. Fluid Mech.* 394 (1999) 51-72.
- [26] P. Le Helley, *Etude theorique et experimentale des instabilites de combustion et de leur controle dans un bruleur premelange*, Ecole Centrale de Paris, (1994).
- [27] A. Kaufmann, F. Nicoud and T. Poinso, *Combust. Flame* 131 (2002) 371-385.
- [28] M. L. Munjal, *Acoustics of Ducts and Mufflers*, John Wiley & Sons, 1986.
- [29] J. E. Ffowcs Williams, *AIAA Journal* 20 (3) (1982) 307-315.
- [30] D. -H. Lee and T. C. Lieuwen, *Acoustical Society of America* 113 (2003) 167-177.
- [31] M. Åbom, *J. Sound Vib.* 155 (1) (1991) 185-188.
- [32] A. G. Doige, M. L. Munjal and H. S. Alves, *Proceedings of Noise-Con 88*, 1988, p. 481-485.
- [33] C. O. Paschereit, W. Polifke, B. Schuermans and O. Mattson, *J. Engng for Gas Turb. and Power* 124 (2002) 239-247.
- [34] M. L. Munjal and A. G. Doige, *J. Sound Vib.* 141 (2) (1990) 323-333.
- [35] T. Sattelmayer, *J. Engng for Gas Turb. and Power* 125 (1) (2003) 11-19.
- [36] T. Sattelmayer and W. Polifke, *Combust. Sci. Tech.* 175 (3) (2003) 453-476.
- [37] T. Sattelmayer and W. Polifke, *Combust. Sci. Tech.* 175 (3) (2003) 477-497.
- [38] J. Eckstein, E. Freitag, C. Hirsch and T. Sattelmayer, *ASME Turbo Expo 2004*, ASME Paper 2004-GT-54163, 2004.
- [39] B. T. Chu, *Proc. Combust. Institute* 4 (1953) 603-612.
- [40] W. Polifke, A. Poncet, C. O. Paschereit and K. Doebbeling, *J. Sound Vib.* 245 (3) (2001) 483-510.
- [41] J. J. Keller, *AIAA Journal* 33 (12) (1995) 2280-2287.
- [42] O. Colin and M. Rudgyard, *J. Comput. Phys.* 162 (2) (2000) 338-371.
- [43] L. Selle, F. Nicoud and T. Poinso, *AIAA Journal* 42 (5) (2004) 958-964.
- [44] T. Poinso and S. Lele, *J. Comput. Phys.* 101 (1) (1992) 104-129.
- [45] M. Baum, T. J. Poinso and D. Thévenin, *J. Comput. Phys.* 116 (1994) 247-261.

## 8 Tables

Transfer matrix coefficients	
$M_{11} =$	$\cos(k_l l)\cos(k_r r) - \Gamma_l (1 + KF(\omega)) \sin(k_l l)\sin(k_r r)$
$M_{12} =$	$i\rho_l c_l (\sin(k_l l)\cos(k_r r) + \Gamma_l (1 + KF(\omega)) \cos(k_l l)\sin(k_r r))$
$M_{21} =$	$\frac{i}{\rho_r c_r} (\cos(k_l l)\sin(k_r r) + \Gamma_l (1 + KF(\omega)) \sin(k_l l)\cos(k_r r))$
$M_{22} =$	$\frac{\rho_l c_l}{\rho_r c_r} (-\sin(k_l l)\sin(k_r r) + \Gamma_l (1 + KF(\omega)) \cos(k_l l)\cos(k_r r))$
with $K = \frac{\gamma-1}{\rho_l c_l^3} \frac{\dot{\Omega}_{T,0}}{S_l}$	

Table 1

Coefficients of the transfer matrix  $\mathcal{M}$  obtained with FTF models.

Cases	Acoustic waves at boundaries	State 1	State 2
Case 1	Forcing is applied		left
	Reflection coefficient	$R_A$	0.1
		$R_E$	0.05
Case 2	Forcing is applied		right
	Reflection coefficient	$R_A$	0.1
		$R_E$	0.05
Case 3	Forcing is applied		left
	Reflection coefficient	$R_A$	0.1
		$R_E$	0.05

Table 2

Set of states used for the calculation of the flame transfer functions. Three cases are chosen for comparisons.

Transfer matrix coefficients
$M_{11} = \cos(k_l l)\cos(k_r r) - \Gamma_l (1 + KF_u(\omega)) \sin(k_l l)\sin(k_r r) \\ + i\gamma\Gamma_l KF_p(\omega)\cos(k_l l)\sin(k_r r)$
$M_{12} = i\rho_l c_l (\sin(k_l l)\cos(k_r r) + \Gamma_l (1 + KF_u(\omega)) \cos(k_l l)\sin(k_r r) \\ + i\gamma\Gamma_l KF_p(\omega)\sin(k_l l)\sin(k_r r))$
$M_{21} = \frac{i}{\rho_r c_r} (\cos(k_l l)\sin(k_r r) + \Gamma_l (1 + KF_u(\omega)) \sin(k_l l)\cos(k_r r) \\ - i\gamma\Gamma_l KF_p(\omega)\cos(k_l l)\cos(k_r r))$
$M_{22} = \frac{\rho_l c_l}{\rho_r c_r} (-\sin(k_l l)\sin(k_r r) + \Gamma_l (1 + F_u(\omega)) \cos(k_l l)\cos(k_r r) \\ + i\gamma\Gamma_l KF_p(\omega)\sin(k_l l)\cos(k_r r))$
with $K = \frac{\gamma-1}{\rho_l c_l^3} \frac{\dot{\Omega}_{T,0}}{S_l}$

Table 3  
Coefficients of the transfer matrix  $\mathcal{M}$  obtained with extended FTF models.

## List of Figures

- 1 ITM approaches: the flame effect is contained in the matrix of the element where the flame is located. 25
- 2 FTF approaches: the inlet velocity reference is measured at a point  $a$ . 25
- 3 Decomposition of the combustor into two-dimensional sections. 25
- 4 Experimental setup of the burner. The dimensions are given in  $mm$ . 26
- 5 Configuration for numerical simulations of the isolated laminar propane air flame. 26
- 6  $t_1$ ) to  $t_4$ ): Snapshots of heat release contours at different times in the flame pulsation cycle (500 Hz). Underneath: unsteady velocity ( $u'/u_0$ ) at the chamber inlet and heat release ( $\dot{\Omega}'_T/\dot{\Omega}_{T,0}$ ) signals with corresponding snapshots' times. 27
- 7 Structure of the 500 Hz mode in the upstream duct ( $x < 0$  mm) for various reflection coefficients at the outlet  $R_E$  (point E): (a) absolute value of the velocity amplitude, (b) absolute value of the pressure amplitude. 28
- 8 Flame transfer function for the  $n - \tau$  model versus the outlet reflection coefficient  $R_E$  (point E): (a) Amplification factor  $n$ , (b) Time delay  $\tau$ . The experimental results were obtained with perfectly non reflecting outlet ( $R_E \simeq 0$ ). 29
- 9 Flame transfer function for the extended  $n - \tau$  model as a function of the outlet reflection coefficient  $R_E$  for cases 1 and 2 and of the inlet reflection coefficient  $R_A$  for case 3. The velocity and pressure fluctuations are evaluated at point B (300 mm upstream of the chamber). The forcing frequency is 500 Hz. 30
- 10 Flame transfer function for the extended  $n - \tau$  model as a function of the outlet reflection coefficient  $R_E$  for cases 1 and 2 and of the inlet reflection coefficient  $R_A$  for case 3. The velocity and pressure fluctuations are evaluated at point C (29 mm upstream of the chamber). The forcing frequency is 500 Hz. 31

- 11 Flame transfer function for the extended  $n - \tau$  model as a function of the outlet reflection coefficient  $R_E$  for cases 1 and 2 and of the inlet reflection coefficient  $R_A$  for case 3. The velocity and pressure fluctuations are evaluated at point D (inlet plane of the chamber). The forcing frequency is 500 Hz. 32
- 12 Comparison of the transfer matrices  $\mathcal{M}$  obtained by the ITM approaches and extended FTF models. 33
- 13 The four coefficients of the transfer matrix  $\mathcal{M}$  of the burner for different positions of the reference point  $x_a$ . Solid line: absolute value; dashed line: phase [rad]. Line and symbols: ITM; line: extended FTF (using the  $n - \tau$  model). 33

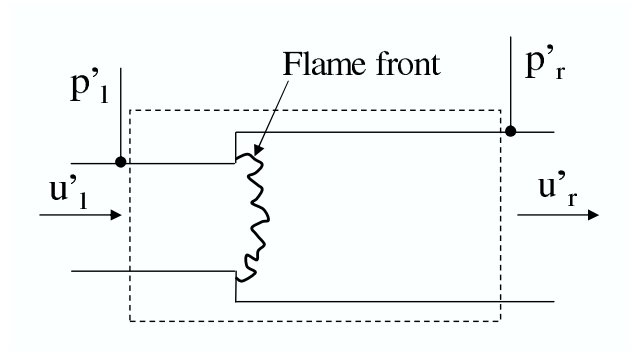


Fig. 1. ITM approaches: the flame effect is contained in the matrix of the element where the flame is located.

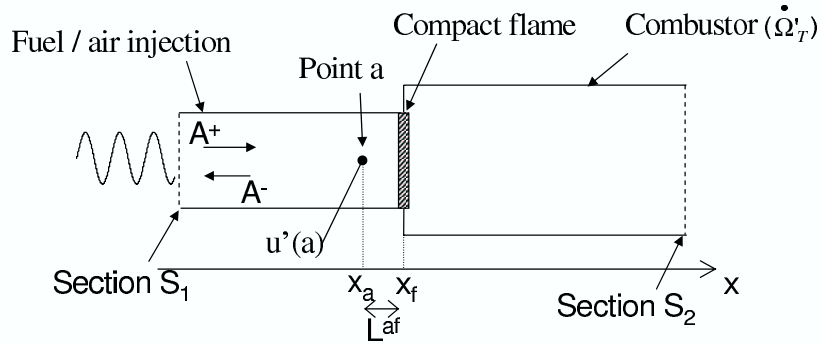


Fig. 2. FTF approaches: the inlet velocity reference is measured at a point  $a$ .

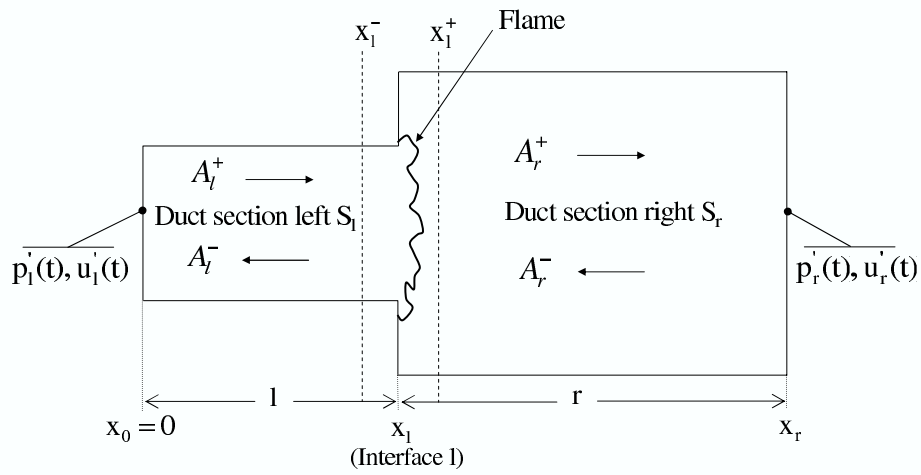


Fig. 3. Decomposition of the combustor into two-dimensional sections.

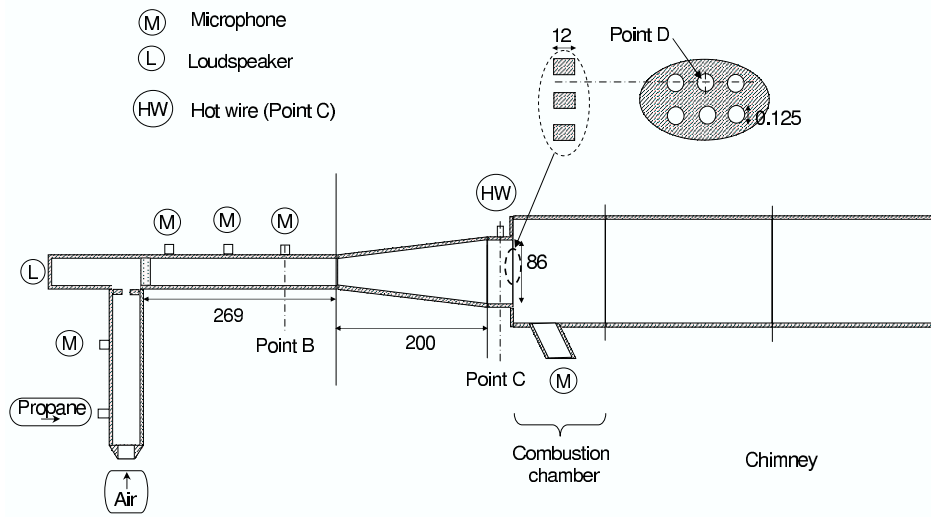


Fig. 4. Experimental setup of the burner. The dimensions are given in *mm*.

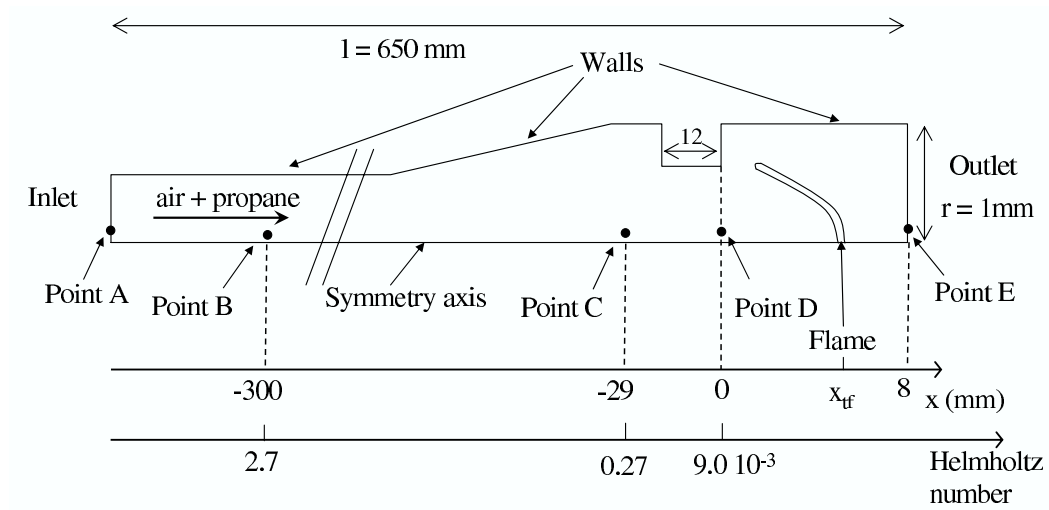


Fig. 5. Configuration for numerical simulations of the isolated laminar propane air flame.

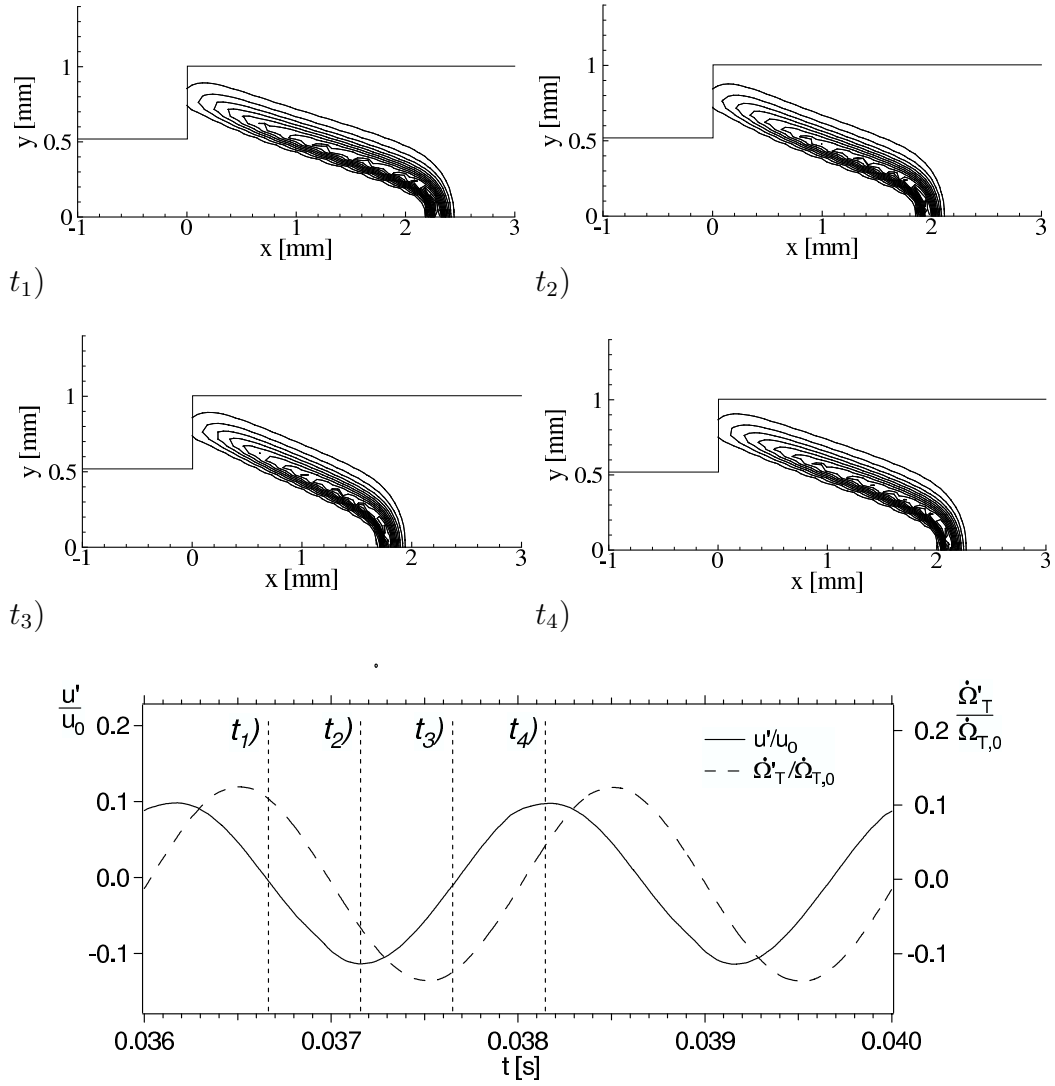


Fig. 6.  $t_1$  to  $t_4$ ): Snapshots of heat release contours at different times in the flame pulsation cycle (500 Hz). Underneath: unsteady velocity ( $u'/u_0$ ) at the chamber inlet and heat release ( $\dot{\Omega}'_T/\dot{\Omega}_{T,0}$ ) signals with corresponding snapshots' times.

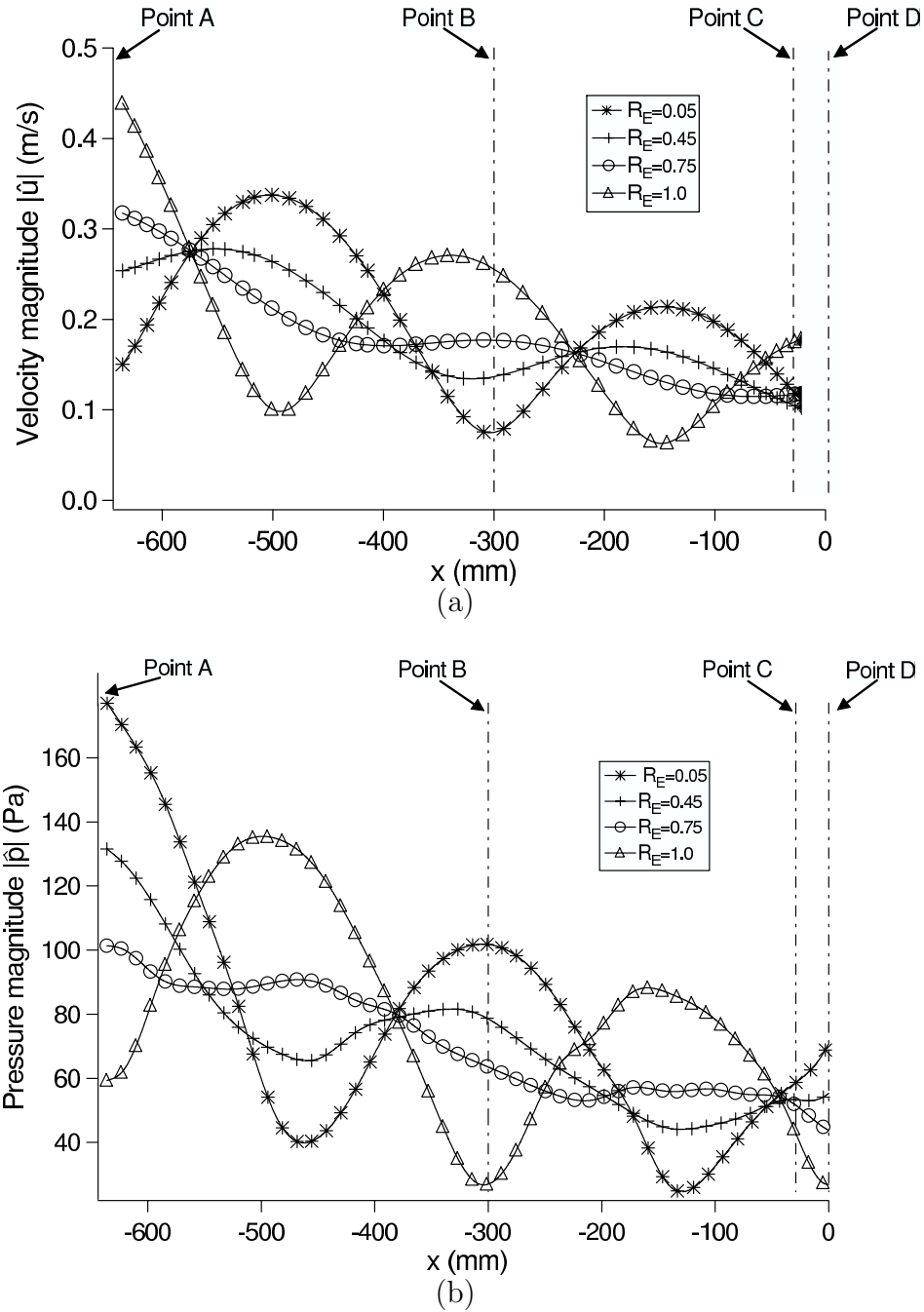
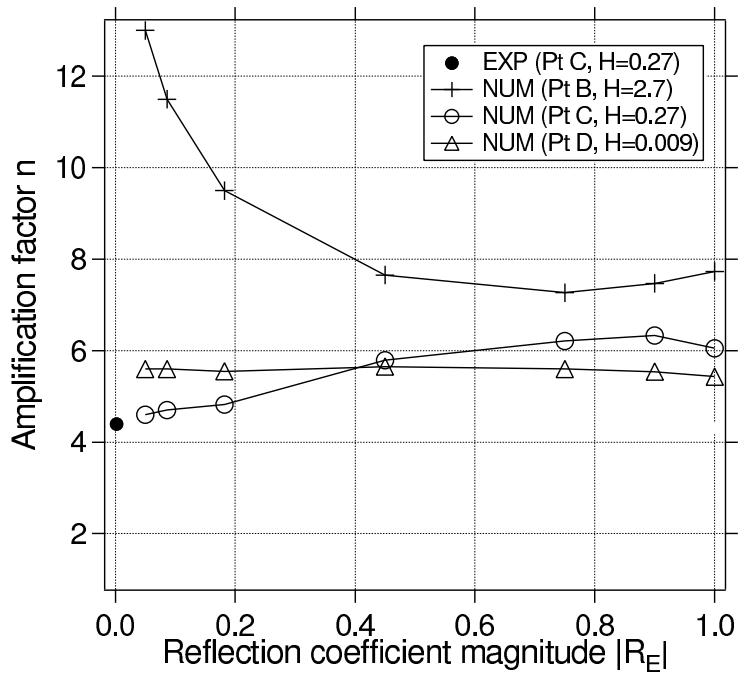
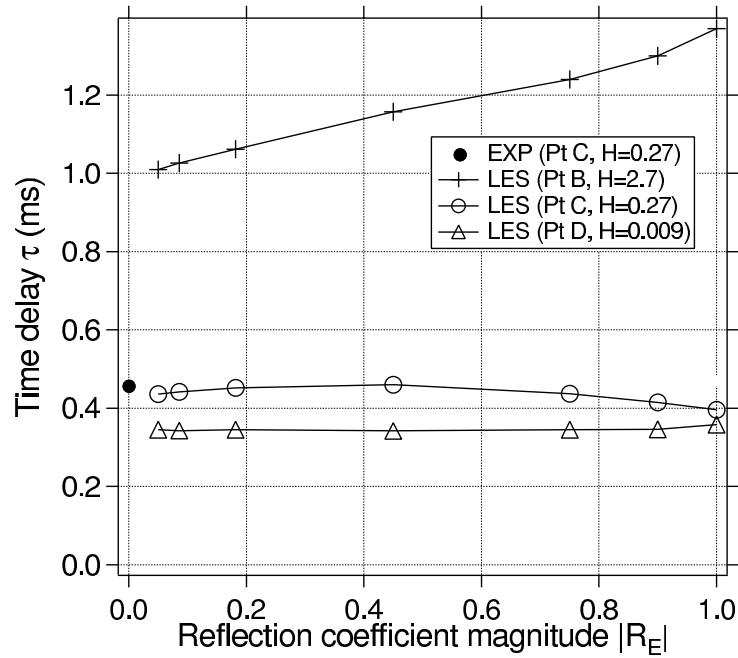


Fig. 7. Structure of the 500 Hz mode in the upstream duct ( $x < 0$  mm) for various reflection coefficients at the outlet  $R_E$  (point E): (a) absolute value of the velocity amplitude, (b) absolute value of the pressure amplitude.



(a)



(b)

Fig. 8. Flame transfer function for the  $n - \tau$  model versus the outlet reflection coefficient  $R_E$  (point E): (a) Amplification factor  $n$ , (b) Time delay  $\tau$ . The experimental results were obtained with perfectly non reflecting outlet ( $R_E \simeq 0$ ).

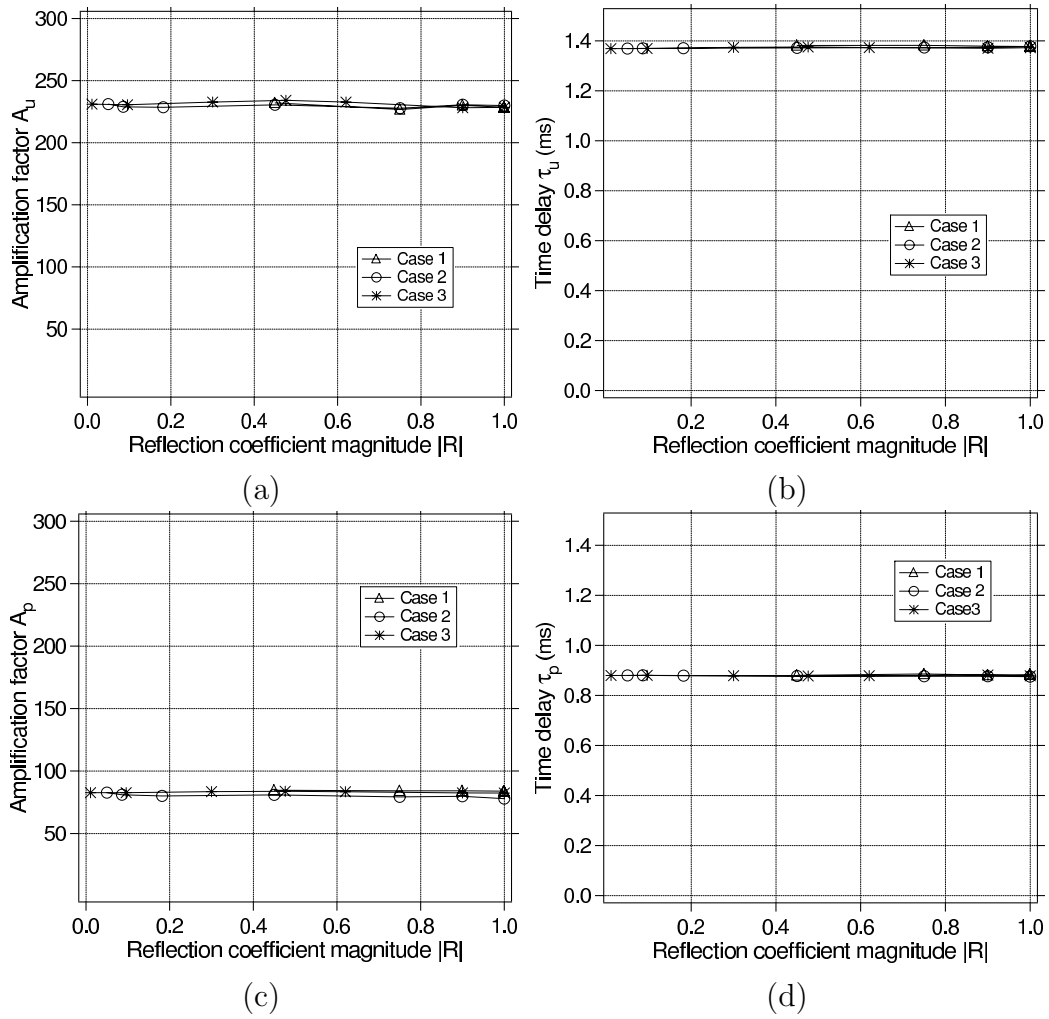


Fig. 9. Flame transfer function for the extended  $n - \tau$  model as a function of the outlet reflection coefficient  $R_E$  for cases 1 and 2 and of the inlet reflection coefficient  $R_A$  for case 3. The velocity and pressure fluctuations are evaluated at point B (300 mm upstream of the chamber). The forcing frequency is 500 Hz.

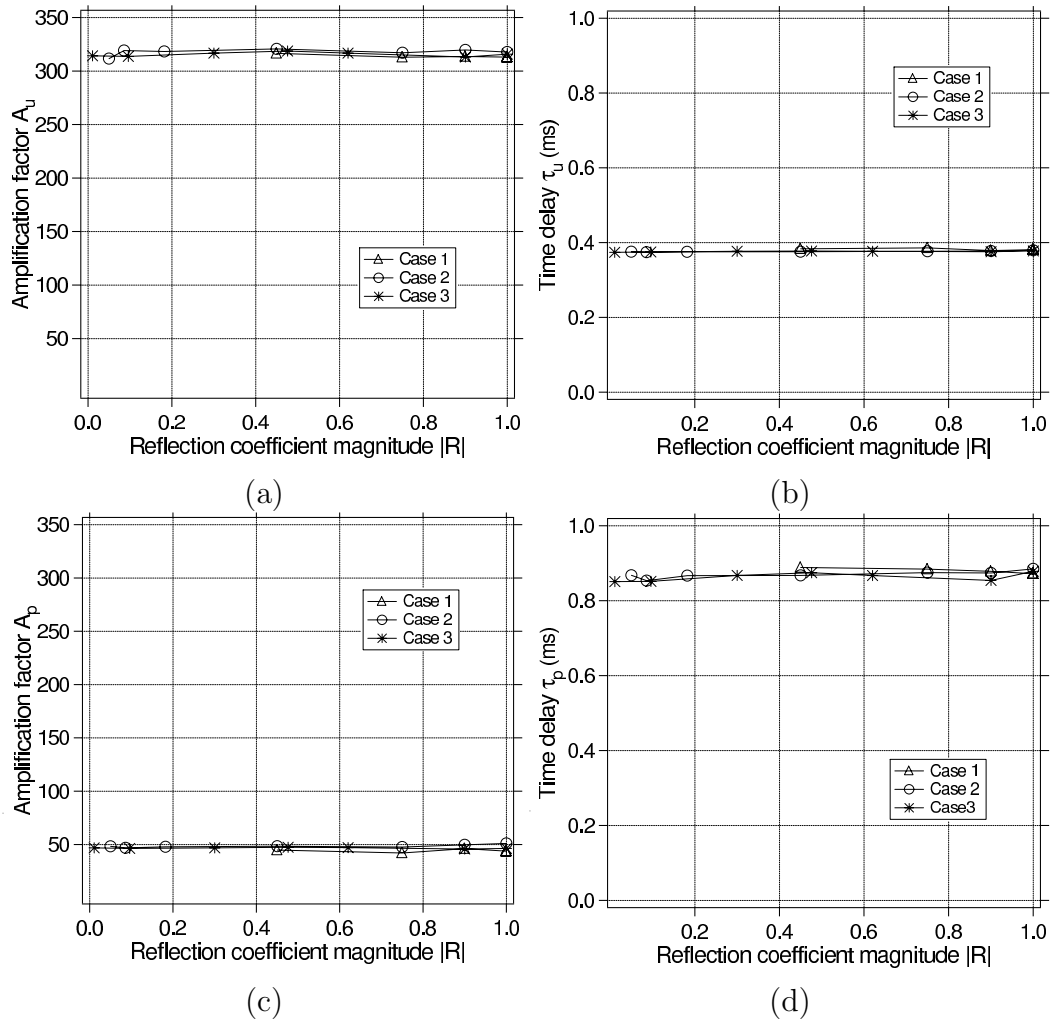


Fig. 10. Flame transfer function for the extended  $n - \tau$  model as a function of the outlet reflection coefficient  $R_E$  for cases 1 and 2 and of the inlet reflection coefficient  $R_A$  for case 3. The velocity and pressure fluctuations are evaluated at point C (29 mm upstream of the chamber). The forcing frequency is 500 Hz.

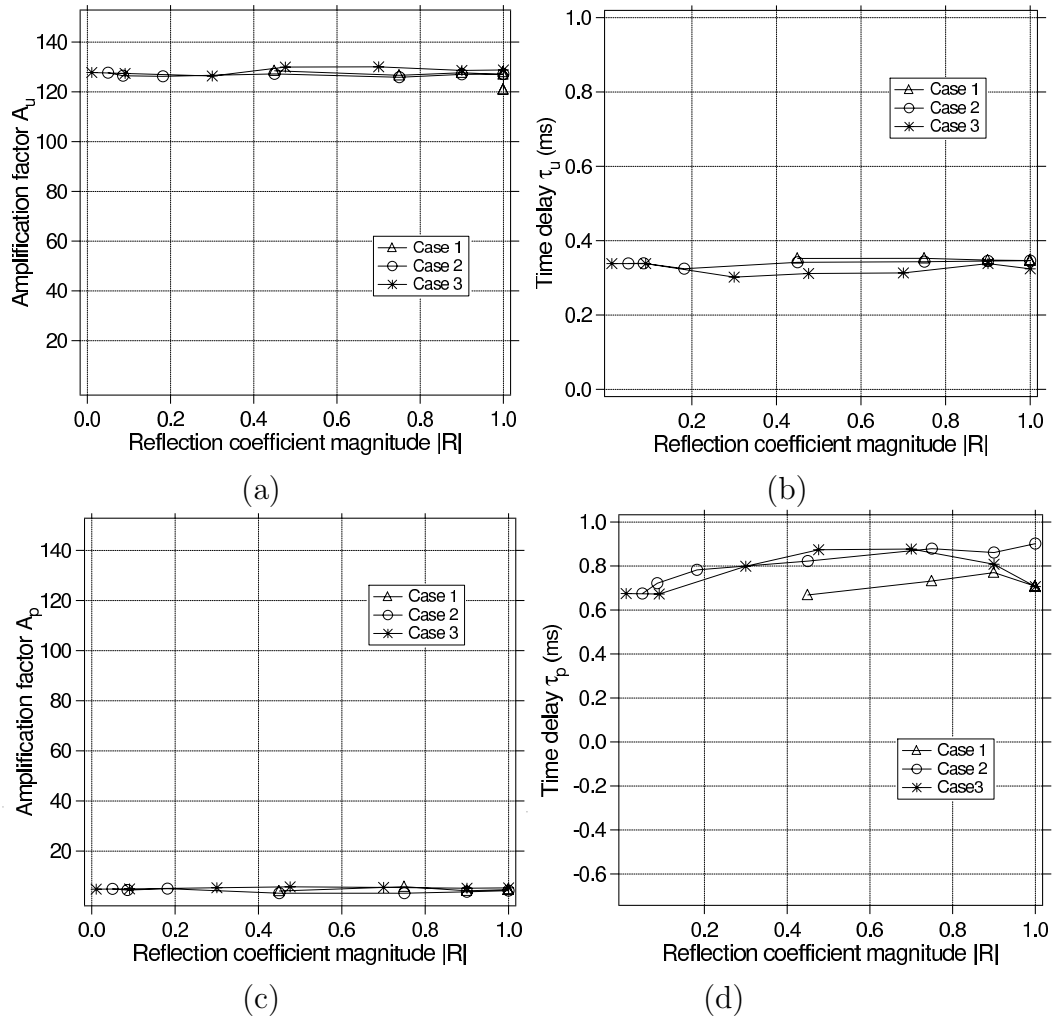


Fig. 11. Flame transfer function for the extended  $n - \tau$  model as a function of the outlet reflection coefficient  $R_E$  for cases 1 and 2 and of the inlet reflection coefficient  $R_A$  for case 3. The velocity and pressure fluctuations are evaluated at point D (inlet plane of the chamber). The forcing frequency is 500 Hz.

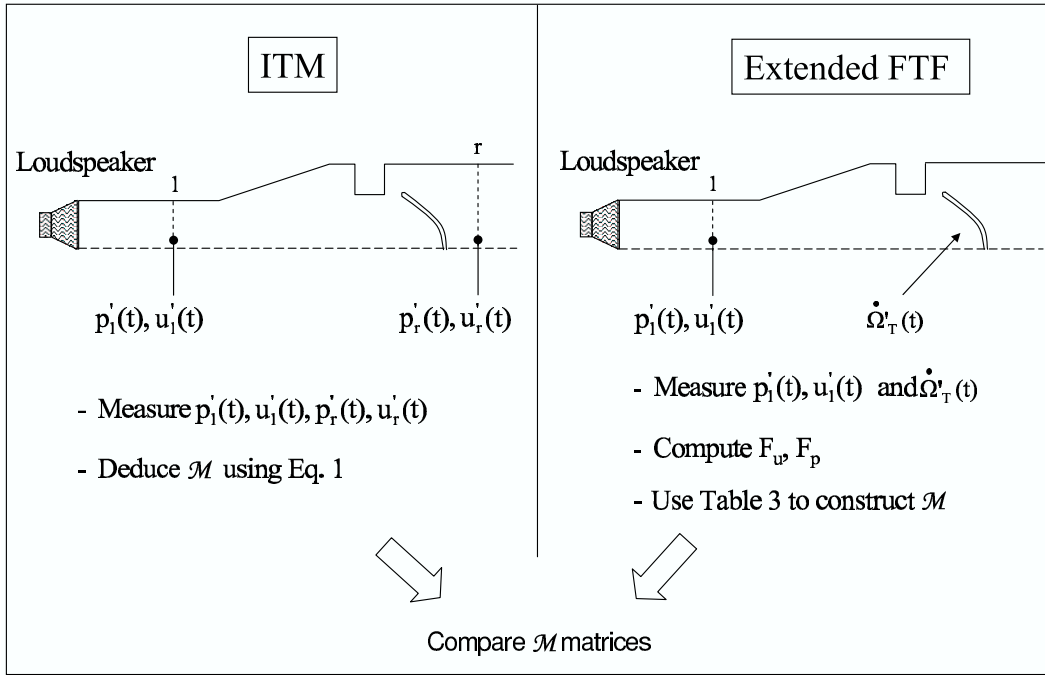


Fig. 12. Comparison of the transfer matrices  $\mathcal{M}$  obtained by the ITM approaches and extended FTF models.

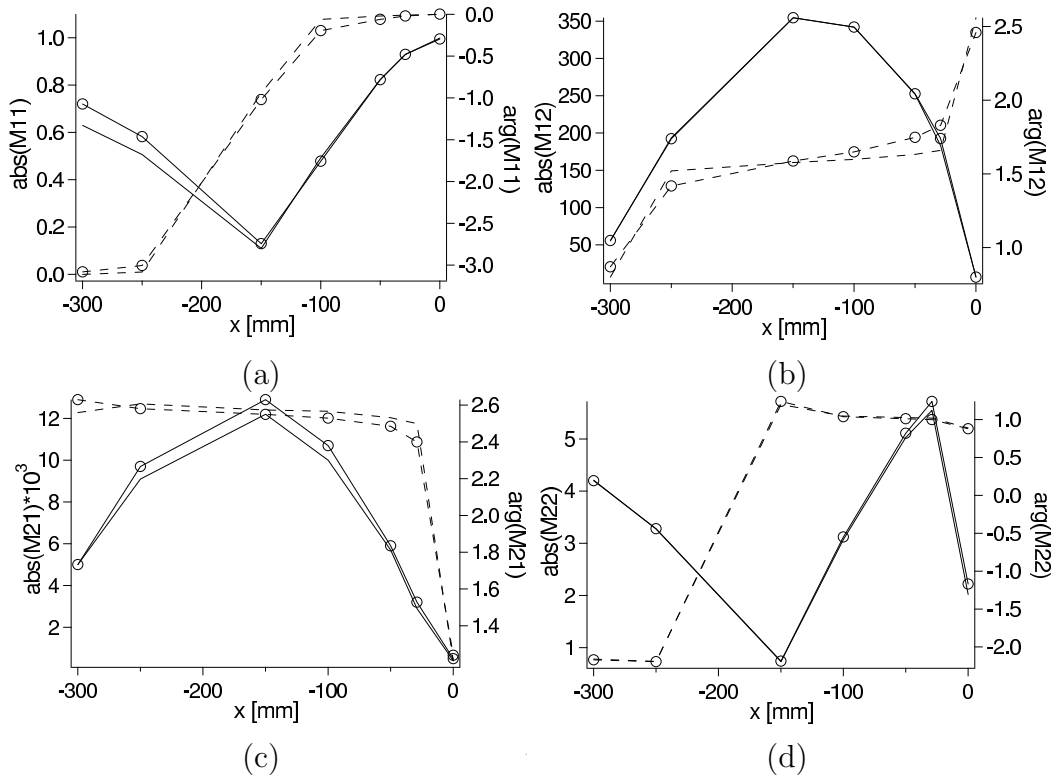


Fig. 13. The four coefficients of the transfer matrix  $\mathcal{M}$  of the burner for different positions of the reference point  $x_a$ . Solid line: absolute value; dashed line: phase [rad]. Line and symbols: ITM; line: extended FTF (using the  $n - \tau$  model).